Journal of the European Ceramic Society 19 (1999) 2931–2940

PII: S0955-2219(99)00055-2
0955-2219/99/$ - see front matter

Comparative Study of Lithium Ion Conductors in the System $Li_{1+x}Al_xA_{2-x}^{IV}(PO_4)_3$ with A^{IV} = Ti or Ge and $0 \leq x \leq 0{\cdot}7$ for Use as Li^+ Sensitive Membranes

M. Cretin and P. Fabry*

Laboratoire d'Electrochimie et de Physico-chimie des Matériaux et des Interfaces, ENSEEG, Associé CNRS (UMR 5631) et Université J. Fourier (Grenoble 1), Domaine Universitaire, BP 75, 38402 Saint Martin d'Hères Cedex, France

(Received 27 October 1997; accepted 21 February 1999)

Abstract

Preparations and physico-chemical characterizations of NASICON-type compounds in the system $Li_{1+x}Al_xA_{2-x}^{IV}(PO_4)_3$ *(*A^{IV} *= Ti or Ge) are described. Ceramics have been fabricated by sol-gel and co-grinding processes for use as ionosensitive membrane for* Li^+ *selective electrodes. The structural and electrical characteristics of the pellets have been examined. Solid solutions are obtained with Al/Ti and Al/Ge substitutions in the range* $0 \leq x \leq 0{\cdot}6$*. A minimum of the rhombohedral* c *parameter appears for* x *about 0·1 for both solutions. The grain ionic conductivity has been characterized only in the case of Ge-based compounds. It is related to the carrier concentration and the structural properties of the NASICON covalent skeleton. The results confirm that the Ti-based framework is more calibrated to* Li^+ *migration than the Ge-based one. A grain conductivity of* 10^{-3} *S* cm^{-1} *is obtained at 25°C in the case of* $Li_{1{\cdot}3}Al_{0{\cdot}3}Ti_{1{\cdot}7}(PO_4)_3$*. A total conductivity of about* 6×10^{-5} *S* cm^{-1} *is measured on sintered pellets because of grain boundary effects. The use of such ceramics in ISE devices has shown that the most confined unit cell (i.e. in Ge-based materials) is more appropriate for selectivity effect, although it is less conductive.*

Keywords: ionic conductivity, sol–gel processes, membranes, lithium ion conductors, ion selective electrodes.

*To whom correspondence should be addressed. E-mail: pierre.fabry@lepmi.inpg.fr

1 Introduction

Fast ionic compounds with 3D NASICON-type framework structures were discovered in the 70s and were synthesized and characterized essentially for energy storage applications.[1,2] They are also promising materials as sensitive membranes, in sensor devices, because they present interesting selectivity properties. They were proposed for such applications in 1984[3,4] and tested for Na^+ potentiometric measurements using $Na_{1+x}Zr_2Si_xP_{3-x}O_{12}$,[5] the optimized composition being $x = 2$–$2{\cdot}2$.[6]

In this way, investigations for lithium ion analysis were made more recently using $Li_{1+x}Al_xTi_{2-x}(PO_4)_3$ (where $x = 0{\cdot}3$ and $x = 0{\cdot}5$).[7,8] However, the selectivity of such NASICON-type Li^+ ceramics against the interfering ions Na^+, K^+, Ca^{2+} and Mg^{2+} (cations present in physiological media) is not sufficient for their use in Ion Selective Electrode (ISE) devices,[7,8] in particular for biomedical applications. As sodium is the principal cation in biological fluids, Na^+ interference must be minimized for such applications.[9]

The NASICON crystallographic structure of $NaA_2^{IV}(PO_4)_3$ (A^{IV} = Ge, Ti and Zr) was identified in 1967–1968.[10] The general formula of NASICON-type compounds is $(M')_n(M'')_m[A_2B_3O_{12}]$ with $n = 0$–1 and $m = 0$–3.[11] The structure can be described as a covalent skeleton $[A_2B_3O_{12}]^-$ constituted of AO_6 octahedra and of BO_4 tetrahedra which form 3D interconnected channels and two types of interstitial spaces (M′ and M″) where conductor cations are distributed. The compounds crystallize with a rhombohedral structure in the R-3C space group, but cell distortions leading to a monoclinic symmetry have been reported.[1,2,11,12] The conductor cations move from one site to

another through bottlenecks of which the size depends on the nature of the skeleton ions and on the carrier concentration in both type of sites (M′ and M″). Consequently, the structural and electrical properties of NASICON-type compounds vary with the composition of the framework. For example in the compounds of general formula $LiA'_{2-x}{}^{IV}A''_{x}{}^{IV}(PO_4)_3$, the cell parameters a and c depend on the A'^{IV} and A''^{IV} cation size.[13] The lowest unit cell has been obtained for $LiGe_2(PO_4)_3$. For improving the Li^+ selectivity of the ISE using Li-NASICON as ceramic membranes, we have undertaken to optimize the composition of such compounds with an unit cell more adapted for selective lithium exchange.

$Li_{1+x}Al_xA_{2-x}{}^{IV}(PO_4)_3$ compounds (with A^{IV} = Ti or Ge) seem to be a good choice and, in the present work, a comparative study of such materials based on Ti and Ge is described. The morphological properties of the materials were examined by scanning electron microscopy and thermogravimetric analysis, the structure by X-ray diffraction and the electrical properties by impedance spectroscopy. The materials have been fabricated mainly by a sol–gel process because the main advantage of such a route is the preparation of very reactive powders having good sintering capabilities. A comparison with a classical co-grinding route is made for $Li_{1+x}Al_xTi_{2-x}(PO_4)_3$ compounds. The characteristics of ion sensitivity and selectivity are reported in details elsewhere.[9] In the present paper only main results concerning the selectivity will be mentioned and discussed.

2 Powder Synthesis and Ceramic Elaborations

Published results concerning such materials have usually related to materials prepared by a co-grinding method.[13–18] The quality of samples (porosity and grain boundary phase) seems to play a major role in the conductive properties.[15–18] Therefore, a sol–gel method was developed for the preparation of $Li_{1+x}Al_xTi_{2-x}(PO_4)_3$ ($x=0$ and 0·3)[7] and we have extended such a process for Ge-based compounds. A detailed description of the preparation has been reported elsewhere[7] and only the main steps are given below.

2.1 Sol–gel powders

The reactants are titanium, germanium and aluminum alkoxides ($Ti(OC_4H_9)_4$ Janssen® 99% pure, $Ge(OC_2H_5)_4$ Strem® 99·99% pure and $Al(OC_4H_9)_3$ Janssen® 97% pure) and lithium and ammonium salts ($CH_3COOLi + 2H_2O$ Strem® 98% pure and $NH_4H_2PO_4$ Fluka® >99% pure). The synthesis steps are given in Fig. 1. A high hydrolysis ratio [$h = [H_2O]/[A(OR)_n]$, where $A(OR)_n$ = alkoxide] was used ($h \approx 400$). In the presence of water excess, hydrolysis polycondensation reactions occur and colloidal precipitates are formed. Our procedure differs on three points from those described by Tohge *et al.*[19] and Ando *et al.*,[20] for $LiTi_2(PO_4)_3$ and $Li_{1.3}Al_{0.3}Ti_{1.7}(PO_4)_3$, respectively:

- a high hydrolysis ratio is used,
- $NH_4H_2PO_4$ instead of $PO(OC_2H_5)_3$, for avoiding precipitation of $TiO(PO_4)_2$, is chosen,
- and the product is dried by freeze drying to avoid agglomeration.[7]

2.2 Co-grinding powders

Li_2CO_3 (Janssen® 99% pure) Al_2O_3 (Baikowski® 99·99% pure), TiO_2 (Merck® 99% pure) and $(NH_4)_2HPO_4$ (R.P.® 99% pure) were used as the starting materials. The stoichiometric mixtures were ground for about 100 h in ethanol with zirconia grinding balls. Then the dried powder was calcined for 2 h at 900°C and ground again. The last steps (calcination and grinding) were repeated twice as indicated by Aono *et al.*[15]

2.3 Ceramic fabrication

Powders were pressed into pellets. The used isostatic pressure was 2500 bars (sol–gel powders) and 3500 bars (co-ground powders). The shrinkage

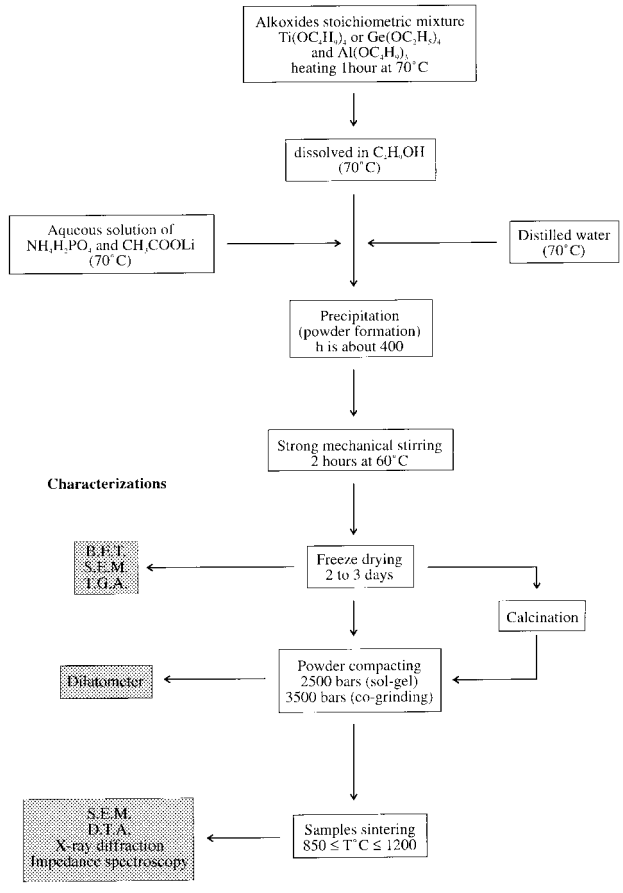

Fig. 1. Li^+-NASICON sol–gel synthesis flow diagram.

(dilatometer Adamel Lhomargy® D.I.24) was monitored, as a function of temperature, for each composition to allow the optimization of the sintering conditions (heating rate, sintering temperature) as described elsewhere.[7] In the case of the sol–gel route, the powders have to be calcined (about 500°C, depending on the composition) before pressing (see Fig. 1). This permits to burn off residual organic groups and to avoid ceramic cracks. The different materials elaborated in this study are given in Table 1. The synthesis process, the temperature and the duration of the sintering stage have also been included. Chemical analyses (S.C.A., C.N.R.S., Vernaison, France) have allowed to verify the composition of the materials (Table 2). The determined composition generally agrees better with the stoichiometric formula in the case of sol–gel ceramics. For $LiTi_2(PO_4)_3$, the error in the lithium content, compared to the stoichiometric value, is 14% for the co-ground material and only 3% for the sol–gel one.

3 Physico-chemical Characterizations of Powders and Ceramics

3.1 Experimental

The thermogravimetric analyser (T.G.A.) was coupled to a Netsch® Simultaneous Thermal Analyser STA 409. The heating rate was 1°C min^{-1}. The microscopic analysis was carried out by SEM (JEOL® JSM 6400).

The powder specific areas were determined by BET (Micromeritics® 2100E1) using N_2 as adsorbed gas, the samples being degased at 150°C.

The structural analysis was conducted with a Siemens® D500 $\theta/2\theta$ diffractometer using $K_{\alpha 1}$ Cu radiation ($\lambda = 0{\cdot}15406$ nm). The cell parameters were calculated with the soft Win-Metrics® (Siemens). High purity silicon was mixed with the powder sample as internal standard.

The crystallization temperatures of ceramics were determined by DTA (Setaram® MDTA 85) with a heating rate of 10°C min^{-1}.

Impedance spectroscopy (impedance analyser HP® 4192 ALF) was used for the electrical characterizations. The frequency range was 13 MHz–5 Hz and the voltage amplitude was 100 mV. The measurements were performed under a primary vacuum between 200 and 25°C on pellets covered with Au blocking electrodes which were deposited using an Edwards® Coating System E 306A evaporator.

Table 1. Synthesis processes and sintering parameters of the compounds

Composition	*Synthesis process*[a]	*Sintering*
$LiTi_2(PO_4)_3$	CG	1100–1200°C (2 h)
	SG	950°C (4 h)
$Li_{1.1}Al_{0.1}Ti_{1.9}(PO_4)_3$	SG	1050°C (2 h)
$Li_{1.3}Al_{0.3}Ti_{1.7}(PO_4)_3$	CG	1000°C (2 h)
	SG	1000°C (2 h)
$Li_{1.5}Al_{0.5}Ti_{1.5}(PO_4)_3$	SG	1000°C (2 h)
$Li_{1.6}Al_{0.6}Ti_{1.4}(PO_4)_3$	SG	950°C (4 h)
$Li_{1.7}Al_{0.7}Ti_{1.3}(PO_4)_3$	SG	950°C (2 h)
$LiGe_2(PO_4)_3$	SG	900°C (4 h)
$Li_{1.1}Al_{0.1}Ge_{1.9}(PO_4)_3$	SG	1050°C (1 h)
$Li_{1.3}Al_{0.3}Ge_{1.7}(PO_4)_3$	CG	950°C (2 h)
	SG	950°C (2 h)
$Li_{1.5}Al_{0.5}Ge_{1.5}(PO_4)_3$	SG	850°C (2 h)
$Li_{1.6}Al_{0.6}Ge_{1.4}(PO_4)_3$	SG	850°C (2 h)
$Li_{1.7}Al_{0.7}Ge_{1.3}(PO_4)_3$	SG	875°C (4 h)

[a]CG: co-grinding process; SG: sol–gel process.

3.2 Results and discussions

3.2.1 Morphological properties

The sol–gel route leads to find ceramics with grain size higher than for the co-ground materials (Fig. 2). This is due to the fine granulometry of the sol–gel powders (0·2 to 0·4 μm in diameter) and the associated high reactivity.

The nature of the alkoxide ($Ti(OC_4H_9)_4$ or $Ge(OC_2H_5)_4$) modifies the morphology of the raw powders ($LiTi_2(PO_4)_3$ or $LiGe_2(PO_4)_3$) (Fig. 3). Figure 4 represents the thermogravimetric results. Below 150°C, a 7% weight loss for both types of product is attributed to residual solvent evaporation (alcohol and water). At higher temperature, a faster and more significant weight loss is observed for $LiGe_2(PO_4)_3$. The high hydrolysis susceptibility of transition metal alkoxides is well known[21] and because of the high hydrolysis rate this might explain a finer grain size of $LiTi_2(PO_4)_3$ compared

Table 2. Elementary analysis of (a) $Li_{1+x}Al_xTi_{2-x}(PO_4)_3$ and (b) $Li_{1+x}Al_xGe_{2-x}(PO_4)_3$ % error in comparison with stoichiometric values (x)

(a)	$Li_{1+x}Al_xTi_{2-x}(PO_4)_3$							
x	*0*		*0·1*	*0·3*		*0·5*	*0·6*	*0·7*
Synthesis	*CG*[a]	*SG*[a]	*SG*	*CG*	*SG*	*SG*	*SG*	*SG*
Li	−14	+3	−9	−11·5	+2·5	−9	−8	−7
Al	—	—	+21·5	−17·5	+1	−4	+4	+1
Ti	—	—	−5	−1·5	−10	−9	−4	−4
P	—	—	−5	−12	−18·5	−9	−1·5	−4
O	—	—	−7·5	−8	−4	−4	+0·2	−1

(b)	$Li_{1+x}Al_xGe_{2-x}(PO_4)_3$					
x	*0*	*0·1*	*0·3*	*0·5*	*0·6*	*0·7*
Synthesis	*SG*	*SG*	*SG*	*SG*	*SG*	*SG*
Li	−0·5	−9·5	−8	+7	−3	−3
Al	—	+9·5	+7	+2·5	−0·2	−2·5
Ge	−6	−7·5	−0·2	−6	−4·5	−12·5
P	−5	−4	−1·5	−0·7	−1	−1·5
O	−8	+5	−8·5	−9·5	−8	−4

[a]CG: co-grinding process; SG: sol–gel process.

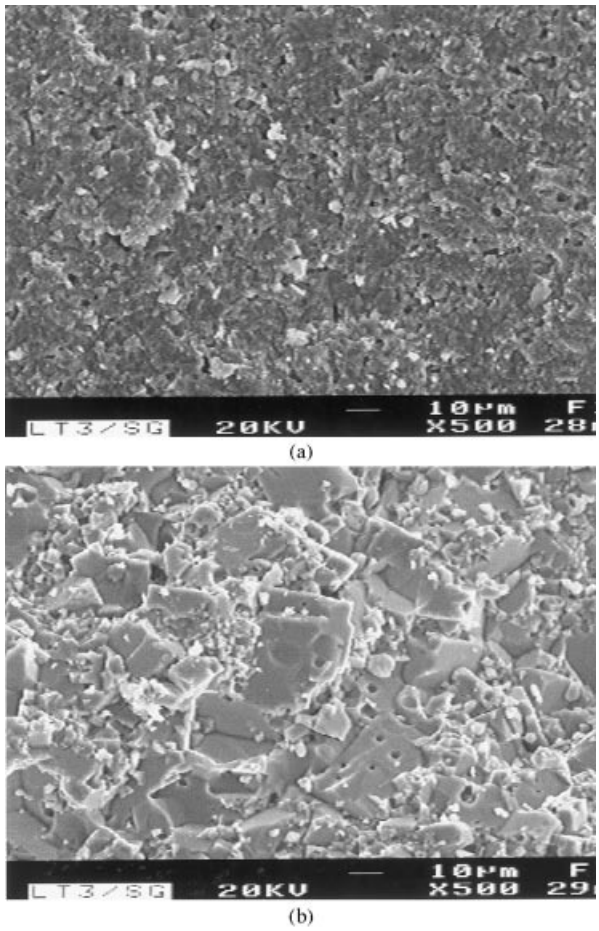

Fig. 2. SEM micrographies. $Li_{1.3}Al_{0.3}Ti_{1.7}(PO_4)_3$ broken pellets, synthesized: (a) by co-grinding; (b) by sol–gel.

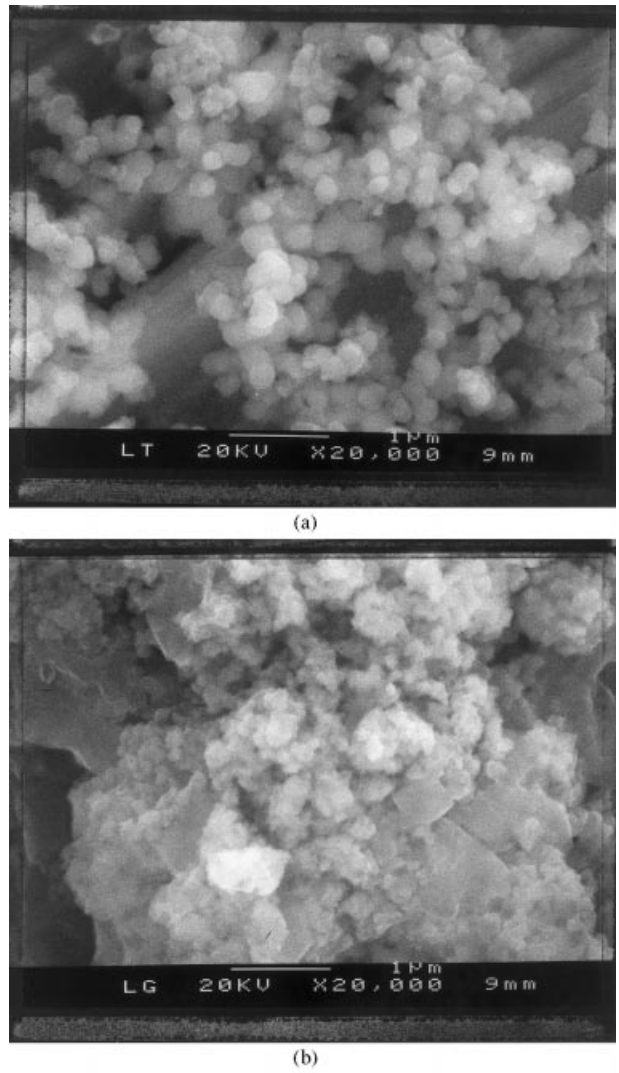

Fig. 3. SEM micrographies of sol–gel powders: (a) $LiTi_2(PO_4)_3$; (b) $LiGe_2(PO_4)_3$.

to $LiGe_2(PO_4)_3$. The higher matter evaporation observed for $LiGe_2(PO_4)_3$ is due to the presence of organic groups in the gel which would have not been eliminated during the condensation reactions because of the slow $Ge(OC_2H_5)_4$ hydrolysis.

3.2.2 Structural properties

The crystallization temperatures of the sol–gel materials have been studied by thermal analysis. They are identified by an exothermic peak on the diagrams and are given in Table 3. The aluminum doping causes a significant decrease in the crystallization temperature. It is due to the decrease in the melting temperature with the increase in the x value observed on $Li_{1+x}Al_xGe_{2-x}(PO_4)_3$.[14]

The symmetry is rhombohedral with a R-3C space group. General results for the cell parameters refinement (hexagonal unit) are summarized in Table 4 for $Li_{1+x}Al_xTi_{2-x}(PO_4)_3$. They are in accordance with literature data for $x=0$.[15,23]

$Li_{1+x}Al_xTi_{2-x}(PO_4)_3$ samples were synthesized to a satisfying fraction of the theoretical density (85 to 93%). As can be seen from the X-ray diffraction analyses (Fig. 5), the compounds $Li_{1.3}Al_{0.3}Ti_{1.7}(PO_4)_3$ elaborated either by co-grinding or by sol–gel seem to be single-phase materials.

The hexagonal unit cell parameters a and c of $Li_{1+x}Al_xTi_{2-x}(PO_4)_3$ are shown in Fig. 6(a). The a parameter decreases with increasing the x values as has also been reported by Aono *et al.*[15] The c parameter passes through a minimum at $x=0{\cdot}1$ and then increases with x up to $x\leq 0{\cdot}6$, contrary to

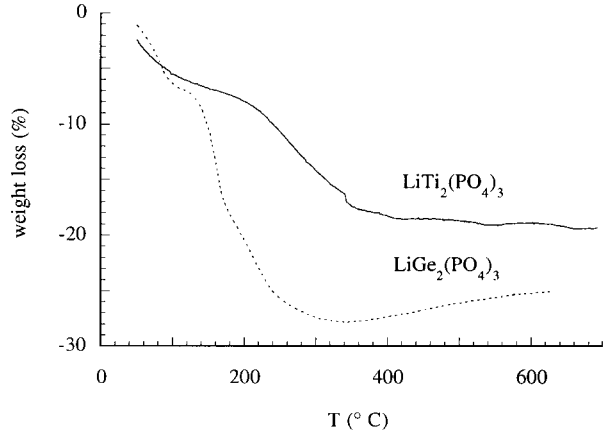

Fig. 4. Thermogravimetric analysis of $LiA_2(PO_4)_3$ (A = Ti and Ge) powders. The heating rate is $1°C\,min^{-1}$.

Table 3. Crystallization temperature of sol–gel materials, DTA, heating rate 10°C min^{-1}

	x					
Composition	*0*	*0·1*	*0·3*	*0·5*	*0·6*	*0·7*
$Li_{1+x}Al_xGe_{2-x}(PO_4)_3$	605	600	610	570	600	575
$Li_{1+x}Al_xTi_{2-x}(PO_4)_3$	720	685	655	650	640	630

Aono *et al.*[15,16] who observed a decrease in the range $0 \leq x \leq 0{\cdot}4$.

Aono *et al.*[16] obtained single phase compounds for $x \leq 0{\cdot}3$ only. In the present results, $Li_{1+x}Al_xTi_{2-x}(PO_4)_3$ sol–gel samples are single-phase materials for $0 \leq x \leq 0{\cdot}6$. Such results may be attributed to the synthesis method, similarly to the synthesis of $LiZr_2(PO_4)_3$ obtained in single phase only when it is elaborated by sol–gel route, as mentioned by Winand *et al.*[13] For $x = 0{\cdot}7$, aluminum phosphates and oxides precipitate and splitting of some diffraction peaks was observed. The latter has been attributed to a structure distortion due to a high doping rate (high x value). Aono *et al.*[15] have also observed such a distortion when x exceeded the solubility limit of the doping cation in the $LiTi_2(PO_4)_3$ phase. In that case the structure changes from a rhombohedral to a monoclinic symmetry.

Results were less satisfying with $Li_{1+x}Al_xGe_{2-x}(PO_4)_3$ sol–gel samples due to the presence of a GeO_2 precipitated phase regardless of the value of x. Moreover the samples were less dense (between 70 and 90%), without any correlation with the x value. The hexagonal unit cell lattice parameters are shown in Fig. 6(b). Our data are consistent with the literature ones for $x = 0$.[13,24] For $x = 0{\cdot}7$, the formation of aluminum phosphates was detected. Splitting of the (1-0-4) diffraction peak was observed for $0 \leq x \leq 0{\cdot}7$. The resulting diffraction line has been described in published works[17] and indexed to the $LiGe_2(PO_4)_3$ phase. However, not all authors have detected this effect.[14] No

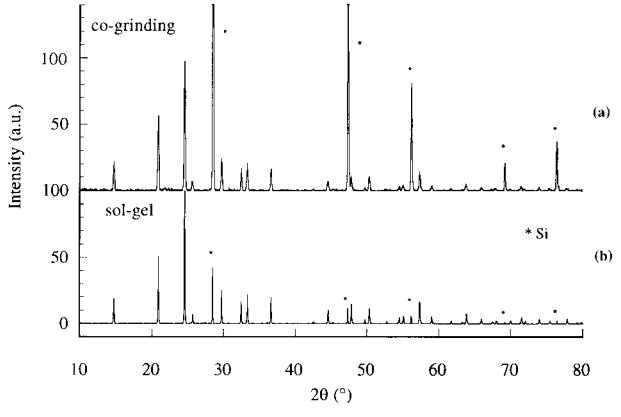

Fig. 5. X-ray diffractograms of $Li_{1{\cdot}3}Al_{0{\cdot}3}Ti_{1{\cdot}7}(PO_4)_3$: (a) co-grinding sample (sintered at 950°C); (b) sol–gel sample (sintered at 950°C).

Table 4. Cell parameters (hexagonal unit) of $Li_{1+x}Al_xTi_{2-x}(PO_4)_3$ as a function of the composition and the synthesis process (the absolute errors are quoted in parentheses)

Composition	*Synthesis*	a *(Å)*	c *(Å)*
$LiTi_2(PO_4)_3$	Co-grinding	8·514 (10^{-3})	20·870 (4×10^{-3})
	Sol–gel	8·5128 (4×10^{-4})	20·868 (3×10^{-3})
	Co-grinding[22]	8·518 (5×10^{-3})	20·87 (10^{-2})
	Co-precipitation (single crystal)[23]	8.517 (2×10^{-3})	20·868 (7×10^{-3})
	Co-grinding[15]	8·512	20·858
$Li_{1{\cdot}3}Al_{0{\cdot}3}Ti_{1{\cdot}7}(PO_4)_3$	Co-grinding	8·504 (10^{-3})	20·881 (4×10^{-3})
	Sol–gel	8·498 (10^{-3})	20·897 (8×10^{-3})
	Co-grinding[15]	8·50	20·808

significant variation of the a parameter as a function of x was observed on our samples. The variations in the c parameters were analogous to those found for the Ti-based compounds.

As a first conclusion, the X-ray diffraction study shows clearly that the solubility limit of Al in the Li^+-NASICON frameworks $LiA_2(PO_4)_3$ (A = Ti or Ge) is about 30 mol% depending on A and hence $Li_{1+x}Al_xA_{2-x}(PO_4)_3$ (A = Ti or Ge) can be considered as solid solutions in the range $0 \leq x \leq 0{\cdot}6$. Analogous conclusions were done by Li *et al.*[14] for A = Ge when Aono *et al.*[16] obtained single phase compounds for $x \leq 0{\cdot}3$ only.

The a parameter evolutions can be interpreted as a qualitative function of the ionic radius of the

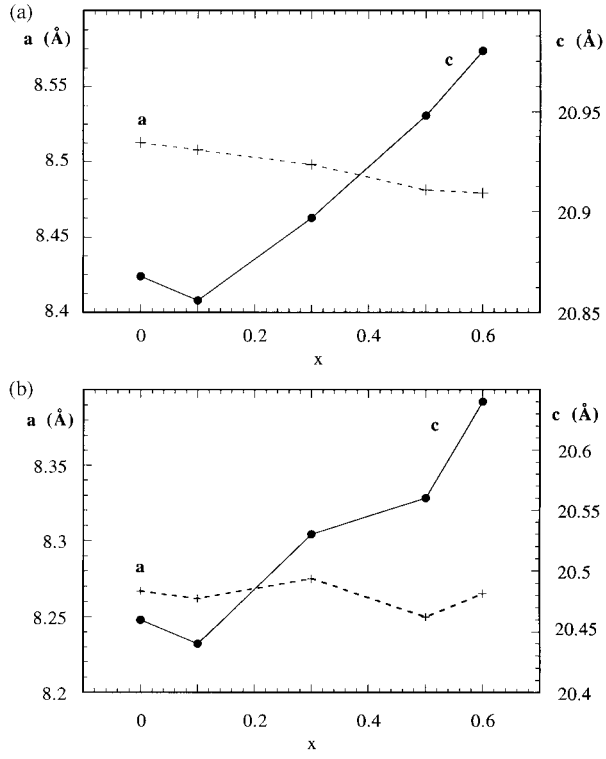

Fig. 6. Cell parameters (hexagonal unit) for: (a) $Li_{1+x}Al_xTi_{2-x}(PO_4)_3$; (b) $Li_{1+x}Al_xGe_{2-x}(PO_4)_3$.

Table 5. Ionic radius in octahedrical position[25]

	Ionic radius (Å)
Al^{3+}	0·535
Ti^{4+}	0·605
Ge^{4+}	0·530

cation in octahedral sites (as memorandum in Table 5 from Ref. 25) since the Al/Ti substitution leads to a decrease of this parameter and for the Al/Ge substitution it remains constant. On this point our results are consistent with those obtained by Li *et al.*[14] and Aono *et al.*[15,16]

The *c* parameter evolutions were also explained by steric effects by Aono *et al.*[15] for $Li_{1+x}Al_xTi_{2-x}(PO_4)_3$. Such an explanation must be improved because for both types of substitution we have observed a minimum for $x = 0{\cdot}1$ and an increase of *c* for $0{\cdot}1 < x < 0{\cdot}6$. Several phenomena play a determinant role in the influence of the cationic substitution on the structure.[26] Such an increase could be attributed to the new occupancy of the conduction sites when the Al^{3+} doping (and consequently Li^+ doping) takes place. During the substitution, the additional Li^+ ions are localized in the M″ sites and this leads to a minimal occupancy of the M′ sites and consequently to a maximal repulsion along the *c* axis as in Na^+-NASICON materials.[2] Our results seem to indicate that the M″ occupancy is the principal effect in Li^+-NASICON for the higher x values. This is contrary to the $Li_{1+x}Al_xA_{2-x}(PO_4)_3$ results reported by Aono *et al.*[15,16]

Nevertheless it should be noted that regardless of the *x* value, the cell volume is lower for Ge-based compounds due to the lower ionic radius of Ge^{4+} compared to Ti^{4+}. The cell volume decrease is about 6%. It is not very much changed by the Al/A substitution ratio as reported by Li *et al.*[14]

3.2.3 *Electrical properties*

The total conductivity (σ_T), i.e. grain and grain boundary system, was calculated from the total impedance value (R_T) determined from the impedance diagrams (Fig. 7). Arrhenius plots are shown in Fig. 8 for $Li_{1{\cdot}3}Al_{0{\cdot}3}Ti_{1{\cdot}7}(PO_4)_3$ elaborated by the two different processes. At room temperature, σ_T is $10^{-4}\,S\,cm^{-1}$ and $1{\cdot}5\times10^{-5}\,S\,cm^{-1}$ for the co-ground and the sol–gel materials, respectively. Activation energies for the total ionic conductivity are 0·42 and 0·39 eV, respectively. As mentioned before, sintered co-ground pellets show a lower grain size than the sol–gel ones. Hence, the higher conductivity observed with the co-ground samples cannot be linked to an increase of the grain contact area which would lead to a decrease in the intergranular impedance.[27] In the same way than Aono *et al.*[17] explain their results, the lower conductivity observed with sol–gel pellets could be due to the intergranular precipitation of a dispersed phase invisible by X-ray diffraction. In our results this product could be $LiTiOPO_4$ which was identified by Raman scattering spectroscopy[28] in the $Li_{1+x}Al_xTi_{2-x}(PO_4)_3$ sol–gel compounds. A sample of the pure $LiTiOPO_4$ phase was synthesized and does not present observable ionic conduction below 200°C.[28] Furthermore in impedance spectroscopy, the depression angle β increases generally with the material inhomogeneity. So, the higher β value observed on sol–gel samples (−20° compared to −13° on the co-ground pellets) could be due to the presence of the $LiTiOPO_4$ phase at the grain boundaries. No study on the correlation of the quantity of such a phase at the grain boundaries and the blocking effect on the total conductivity was made on those materials, because it would be too consequent and out of our field of investigation

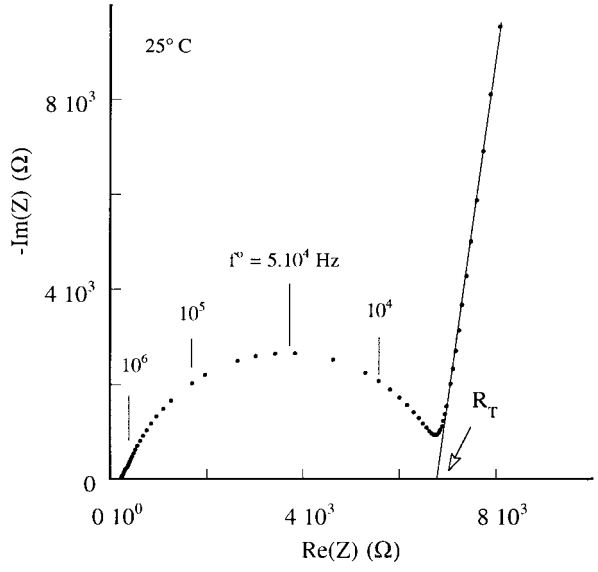

Fig. 7. Impedance diagram obtained at 25°C on a $Li_{1{\cdot}3}Al_{0{\cdot}3}Ti_{1{\cdot}7}(PO_4)_3$ pellet, using Au electrodes.

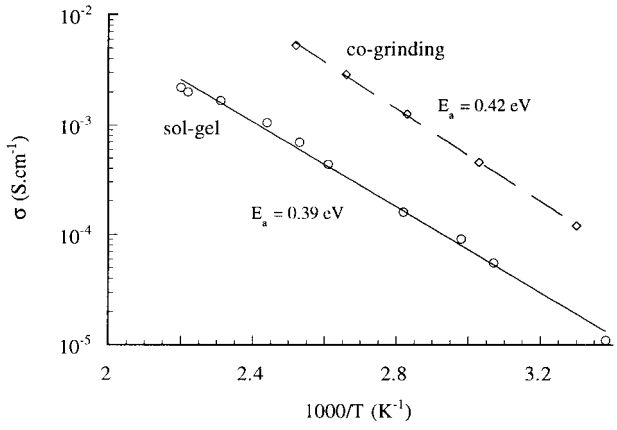

Fig. 8. Arrhenius plots of the total ionic conductivity of $Li_{1{\cdot}3}Al_{0{\cdot}3}Ti_{1{\cdot}7}(PO_4)_3$ synthesized by co-grinding and sol–gel processes.

Table 6. Total ionic conductivity at room temperature and activation energy of the sol–gel materials

		x					
		0	*0·1*	*0·3*	*0·5*	*0·6*	*0·7*
A = Ti	σ_T (S cm^{-1})	$4{\cdot}4\times10^{-8}$*	3×10^{-5}	$1{\cdot}5$ to 6×10^{-5}	—	$2{\cdot}3\times10^{-5}$	$3{\cdot}7\times10^{-5}$
	E_a (eV)	0·51	0·38	0·39	—	0·32	0·36
A = Ge	σ_T (S cm^{-1})	$5{\cdot}9\times10^{-9}$*	$2{\cdot}9\times10^{-6}$	$3{\cdot}9\times10^{-5}$	$2{\cdot}8\times10^{-4}$	$1{\cdot}4\times10^{-4}$	$1{\cdot}5\times10^{-4}$
	E_a (eV)	0·65	0·42	0·40	0·33	0·36	0·36

*Extrapolated value.

(materials for ISE devices). Nevertheless it could be of a fundamental interest.

The total conductivity (σ_T) and the activation energy (E_a) at room temperature as a function of the compositions of the sol-gel materials are given in Table 6. For Ge- and Ti-based materials, σ_T increases with the doping level and hence with the carrier concentration.

The relaxation frequency (determined by $RC\omega^\circ = 1$ at the top of the semicircles in the Nyquist diagrams) as generally reported for pure NASICON phases is higher than 10^5 Hz at room temperature. Thus, the relaxation frequency observed on Fig. 7 is not characteristic of a pure fast ionic conductor. The obtained electrical response is essentially due to blocking effects of the ionic conductivity at the grain boundaries. Therefore an attempt was made to examine the different electrical contributions separately. For $Li_{1{\cdot}1}Al_{0{\cdot}1}Ge_{1{\cdot}9}(PO_4)_3$, the impedance diagram studied after subtraction of the low frequency part (relative to the electrode reaction) is shown on Fig. 9. It allows to determine R_g (grain impedance) and R_{gb} (grain boundary impedance). Arrhenius representations of $1/R_g$, $1/R_{gb}$ and $1/R_T$ are shown in Fig. 10. Activation energies were found to be 0·31 and 0·46 eV for the NASICON-phase conduction and the grain boundary, respectively. These results are in good agreement with these of Aono *et al.*[17] who reported activation energy values of 0·38 and 0·46 eV for these types of conduction. Therefore, as mentioned by these authors, the total conductivity of such materials seems to be limited by blocking effects at the grain boundaries. Aono *et al.*[15–18] have for example noticed the effect of the $Li_3A_2(PO_4)_3$ phase on the porosity and have observed a correlation between the porosity of samples and their conductivity (with a porosity up to 30%).

To characterize this effect, we calculated α_R (blocking factor) for other compositions. α_R is defined by the following relation:[29]

$$\alpha_R = 100 \times \frac{R_{gb}}{R_T} \qquad (1)$$

The α_R values (Table 7) were found to be generally high. For $Li_{1+x}Al_xTi_{2-x}(PO_4)_3$ it was very difficult to separate the grain contribution because its relaxation frequency and the grain boundary one were too close. Hence only α_R values for $x = 0{\cdot}3$ can be compared with those found by Aono for which a calculation gives α_R about 70 for $x = 0{\cdot}5$.[17] In our results, no typical correlation was observed with the density of the samples.

The blocking conductivity effects are due to GeO_2 and $LiTiOPO_4$ phases observed in $Li_{1+x}Al_xGe_{2-x}(PO_4)_3$ by X-ray diffraction and in $Li_{1+x}Al_xTi_{2-x}(PO_4)_3$ by Raman spectroscopy. $LiTiOPO_4$, which is invisible by X-ray diffraction, was found to be definitely more dispersed than GeO_2. As NASICON grain contact areas are lower for $Li_{1+x}Al_xTi_{2-x}(PO_4)_3$ materials, the blocking factor α_R is greater for this type of compound.

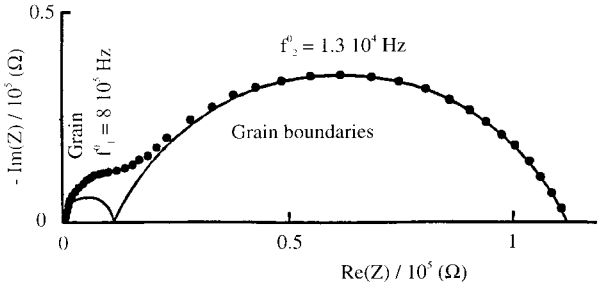

Fig. 9. Impedance diagram at 37°C for $Li_{1{\cdot}1}Al_{0{\cdot}1}Ge_{1{\cdot}9}(PO_4)_3$ obtained with the sol–gel process.

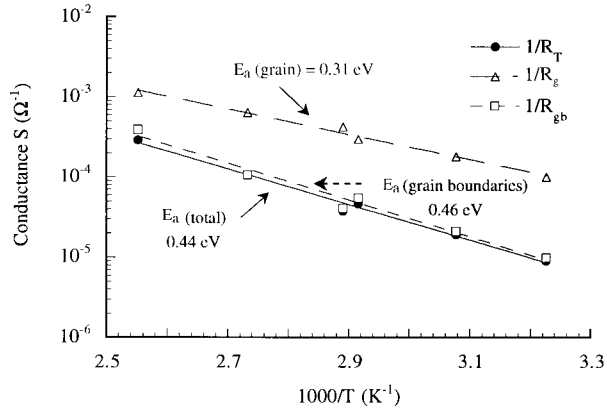

Fig. 10. Arrhenius plots of the grains ($1/R_g$), the grain boundaries ($1/R_{gb}$) and the total ($1/R_T$) conductances of $Li_{1{\cdot}1}Al_{0{\cdot}1}Ge_{1{\cdot}9}(PO_4)_3$ obtained with the sol–gel process.

Table 7. Blocking factor α_R and grain conductivity σ_g of NASICON-type compounds

	$Li_{1+x}Al_xGe_{2-x}(PO_4)_3$				$Li_{1+x}Al_xTi_{2-x}(PO_4)_3$
	x = 0·1 (37°C)	x = 0·3 (26°C)	x = 0·6 (26°C)	x = 0·7 (23°C)	x = 0·3 (24°C)
α_R (%)	91	76	54	79	94
σ_g (S cm^{-1})	$5{\cdot}6\times10^{-5}$	$1{\cdot}6\times10^{-4}$	3×10^{-4}	7×10^{-4}	10^{-3}

The grain conductivity of the NASICON phases was calculated from the R_g values. The geometric factor chosen for these calculations was the one of the pellet. Results are also given in Table 7. $Li_{1+x}Al_xGe_{2-x}(PO_4)_3$ ($0\leq x\leq 0{\cdot}7$) grain conductivity increases with increasing x values, i.e. with Li^+ increasingly occupy the M″ sites. The new charge distribution leads to both a destabilization and a depopulation of the M′ sites thus favoring the ionic conduction. This effect was described previously with Na^+-NASICON.[30]

At $x = 0{\cdot}3$, the grain conductivity of Ti-based NASICON materials is 6-fold higher than the Ge-based ones. These results confirm that the $[Ti_2P_3O_{12}]^-$ framework is much more appropriate for Li^+ migration than the $[Ge_2P_3O_{12}]^-$. The $LiGe_2(PO_4)_3$ crystalline cell, whose parameters are only slightly modified by Al doping, is too small to permit an optimal Li^+ motion.

4 Ionic Selectivity Properties

Potentiometric sensors were fabricated with fast ionic compounds as selective membrane according to the following electrochemical cell:

Ag–AgCl/LiCl 10^{-1} mol l^{-1}/Ionic Conductor/ Analyzed Solution//Ref. Electrode (SCE)

The selectivity properties of Li^+-NASICON have been examined from the values of the potentiometric interference coefficients (also named in the literature 'potentiometric ion selectivity coefficients') $K^{Pot}_{i,j}$ where i is the primary ion and j the interfering ion. The coefficients have been determined by the mixed solution method with a fixed lithium level. Experimental part has been described in details elsewhere.[9] The Nickolskii empirical equation has been used as follows:

$$E = E^\circ + \frac{2{\cdot}3RT}{z_iF}\log\left(a_i + \sum_j\left(K^{Pot}_{i,j}\times a_j^{z_i/z_j}\right)\right) \quad (2)$$

where R, T, z_i, F and a_i are the gas constant, the absolute temperature, the charge of the ion, the Faraday constant and the activity of the ion i (or j), respectively. The $K^{Pot}_{i,j}$ values with j = Na^+ and K^+ are given in Table 8 as a function of the Li^+-NASICON membrane composition. The values show the dependance of the cation size on the selectivity, whatever the Li^+ NASICON composition is. The ionic radii in octahedrical position are 1·38 and 1·02 Å for K^+ and Na^+, respectively (0·76 Å for Li^+)[25] and the $K^{Pot}_{Li,K}$ values are about 10^{-3} whereas the $K^{Pot}_{Li,Na}$ ones are clearly higher ($1{\cdot}6\times10^{-2}$ to 0·65). Another important point is the lower interference of Na^+ in the case of the Ge-based materials. For example for $x = 0{\cdot}3$, the $K^{Pot}_{Li,Na}$ values are 0·65 and $1{\cdot}6\times10^{-2}$ for the Ti- and Ge-based membranes, respectively. Concerning the K^+ interference, the highest $K^{Pot}_{Li,K}$ value is obtained for the Ti-based membrane too. The structural characterization has shown that the Ti/Ge substitution in the $Li_{1+x}Al_xA^{IV}_{2-x}(PO_4)_3$ (with A = Ti or Ge) leads to a decrease of the crystallographic cell volume. The contraction is about 6% in this case.

Such a steric effect on the selectivity is also observable for low variations of the cell parameters in the $Li_{1+x}Al_xGe_{2-x}(PO_4)_3$ family but it is slightly less convincing. According to the values from Fig. 6(b) transferred in Table 8, one can observe a slight increase of $K^{Pot}_{Li,Na}$ versus the c parameter (excepted for the singular point $x = 0{\cdot}1$). The variations of the a parameter are not significant and no obvious effect is observed.

Table 8. Comparison of the interference coefficients as a function of the Li^+-NASICON composition and the cell parameters (a and c in hexagonal unit)

Membrane	x	c (Å)	a (Å)	$K^{Pot}_{Li,Na}$	$K^{Pot}_{Li,K}$
$Li_{1+x}Al_xTi_{2-x}(PO_4)_3$	0·3	20·9	8·5	0·65	8×10^{-3}
	0·5	20·95	8·475	0·45	—
$Li_{1+x}Al_xGe_{2-x}(PO_4)_3$	0·1	20·44	8·26	8×10^{-2}	—
	0·3	20·53	8·273	$1{\cdot}6\times10^{-2}$	5×10^{-3}
	0·5	20·56	8·25	$1{\cdot}8\times10^{-2}$	$3{\cdot}2\times10^{-3}$
	0·6	20·54	8·265	$2{\cdot}3\times10^{-2}$	2.3×10^{-3}
	0·7	—	—	$3{\cdot}1\times10^{-2}$	3×10^{-3}

About the potassium interference, the steric effect is strong because K^+ is a big ion. The value of $K^{Pot}_{Li,K}$ are then smaller and no tendency can be clearly observable for low variations of the unit cell (the fluctuations of $K^{Pot}_{Li,K}$ could be also due to the accuracy of measurement of this parameter for low values).

It must be mentioned that the grain conductivity of the Li^+-NASICON is higher for the $Li_{1\cdot3}Al_{0\cdot3}Ti_{1\cdot7}(PO_4)_3$ membrane than for the $Li_{1\cdot3}Al_{0\cdot3}Ge_{1\cdot7}(PO_4)_3$ one (the values of σ_g is 10^{-3} and $1\cdot6\times10^{-4}\,S\,cm^{-1}$, respectively). It appears clearly that the contraction has a positive effect on the selectivity and a negative effect on the conductivity. The optimal size for the selectivity is smaller than the optimal size for the conductivity by Li^+, i.e. the mobility (the concentrations of mobile ions can be considered constant for the two compositions).

Nevertheless this effect is not a disadvantage for the use of such membranes in potentiometric measurements, because the conductivity values are always very higher than the usual membrane ones. A conductivity of about $10^{-4}\,S\,cm^{-1}$ is confortable when it is compared to those of the usual potentiometric membranes (from 10^{-5} down to $10^{-12}\,S\,cm^{-1}$).

For the proton interference, it was reported elsewhere that the interference process result principally of surface reactions with hydroxide groups.[31,32] The interference is essentially function of the composition and the synthesis method and not a function of the crystalline cell. It was remarked than the H^+ interference is lower for the Li^+-NASICON membrane than for the Na^+-NASICON one which is a compound based on silica involving silanol groups.

5 Conclusion

The sol–gel route has allowed the synthesis of fine ceramic powders (0·2 to 0·4 μm in diameter). It leads to sintered materials of general formula $Li_{1+x}Al_xA_{2-x}{}^{IV}(PO_4)_3$ (A^{IV} = Ti or Ge) having grain size considerably higher than those elaborated by the classical co-ground process.

Both types of substitutions (Al/Ti and Al/Ge) yield solid solutions in the range $x = 0\cdot1$–$0\cdot6$. For $x = 0\cdot7$, aluminium oxides and phosphates precipitate. The variations of the cell parameters a and c (hexagonal unit cell) studied as a function of the doping rate x show that the a value increases with increasing cation ionic radius in the octahedral position (Al^{3+}, Ti^{4+} or Ge^{4+}), whereas the parameter c seems to be related to the conduction site occupation, i.e. the doping content x.

The ionic conductivity of the NASICON-type polycrystalline materials is limited by the blocking effects, caused by the presence of impurities which precipitate at the ceramic grain boundaries. These findings are in accordance with those reported by Aono *et al.*[17] The results of the present study indicate that Li^+-NASICON grain conductivity σ_g depends essentially on the carrier concentration for the Ge-based compounds. Furthermore, at a constant doping content (x), σ_g values of the Ti-based materials are greater than those of the Ge-based ones. Thus, the $[Ti_2P_3O_{12}]^-$ skeleton seems to be better calibrated than $[Ge_2P_3O_{12}]^-$ for Li^+ motion. The Ge-based framework is too confining for optimal lithium migration. Such phenomenon could be a disadvantage for electrochemical cells but not for potentiometric sensor devices.

The more positive point of such a study is that the more confined unit cell is appropriate for selective behaviour in ISE devices, because the mobility of the interfering ion should be considerably lowered, more lowered than the Li^+ one. So, the selectivity coefficient against Na^+ can be improved by a factor higher than one order of magnitude if the Ge-based material is chosen.

Acknowledgements

This work was supported by the "Région Rhône-Alpes" in collaboration with Radiometer Analytical S.A. The authors would thank particularly Mr J. J. Fombon for his advice in this field. They wish to acknowledge the assistance of Mr J. Garden with SEM micrographies. They are grateful to Mr B. Bochu for performing the X-ray diffractions and to Mr M. Hénault for his amicable collaboration.

References

1. Hong, H. P. Y., Crystal structures and crystal chemistry in the system $Na_{1+x}Zr_2Si_xP_{3-x}O_{12}$. *Mat. Res. Bull.*, 1976, **11**, 173–182.
2. Goodenough, J. B., Hong, H. Y. P. and Kafalas, J. A., Fast Na^+ ion transport in skeleton structures. *Mat. Res. Bull.*, 1976, **11**, 203–220.
3. Fabry P., Gros, J. P. and Kleitz, M., Solid state ionics for ISFETs. Symposium on Electrochemical Sensors, Rome, 12–14 June, 1984.
4. Engell, J. and Mortensen, J. S., Ion sensitive measuring device. Radiometer Int. Patent WO 84:01829, 1984.
5. Caneiro, A., Fabry, P., Khireddine, H. and Siebert, E., Performance characteristics of sodium super ionic conductor prepared by sol–gel route for sodium ion sensors. *Anal. Chem.*, 1991, **63**, 2550–2557.
6. Khireddine, H., Fabry, P., Caneiro, A. and Bochu, B., Optimization of NASICON composition for Na^+ recognition. *Sensors and Actuators B*, 1997, **40**, 223–230.
7. Cretin, M., Fabry, P. and Abello, L., Study of Li_{1+x}-$Al_xTi_{2-x}(PO_4)_3$ for potentiometric sensors. *J. Eur. Ceram. Soc.*, 1995, **15**, 1149–1156.
8. Cretin, M. and Fabry, P., Caractérisations de céramiques conductrices pour capteurs potentiométriques à ion lithium. *Ann. Chim. Fr.*, 1995, **20**, 433–438.

9. Cretin, M. and Fabry, P., Detection and selectivity properties of Li^+-ion-selective electrodes based on NASICON-type ceramics. *Anal. Chim. Acta*, 1997, **357**, 291–299.
10. Hagman, L. O. and Kierkegaard, P., The crystal structure of $NaMe^{IV}(PO_4)_3$; Me^{IV} = Ge, Ti, Zr. *Acta Chem. Scand.*, 1968, **22**, 1822–1832.
11. Kreuer, K. D., Kohler, H. and Maier, J., Sodium ion conductors with NASICON framework structure. In *High Conductivity in Solid Ionic Conductor*, ed. T. Takahashi, World Scientific, Singapore, 1989, pp. 242–279.
12. Hamdoune, S., Gondran, M. and Tran Qui, D., Synthesis and crystallographic data for the system $Li_{1+x}Ti_{2-x}In_x(PO_4)_3$. *Mat. Res. Bull.*, 1986, **21**, 237–242.
13. Winand, J. M., Rulmont, A. and Tarte, P., Nouvelles solutions solides $L^I(M^{IV})_{2-x}(N^{IV})_x(PO_4)_3$ (L = Li, Na; M, N = Ge, Sn, Ti, Zr, Hf). Synthèse et étude par diffraction X et conductivité ionique. *J. Solid State Chem.*, 1991, **93**, 341–349.
14. Li, S. C., Cai, J. Y. and Lin, Z. X., Phase relationships and electrical conductivity of $Li_{1+x}Ge_{2-x}Al_xP_3O_{12}$ and $Li_{1+x}Ge_{2-x}Cr_xP_3O_{12}$ systems. *Solid State Ionics*, 1988, **28-30**, 1265–1270.
15. Aono, H., Sugimoto, E., Sadaoka, Y., Imanaka, N. and Adachi, G. Y., Ionic conductivity of solid electrolytes based on lithium titanium phosphate. *J. Electrochem. Soc.*, 1990, **137**, 1023–1027.
16. Aono, H., Sugimoto, E., Sadaoka, Y., Imanaka, N. and Adachi, G. Y., Ionic conductivity of lithium titanium phosphate system. *Solid State Ionics*, 1990, **40/41**, 38–42.
17. Aono, H., Sugimoto, E., Sadaoka, Y., Imanaka, N. and Adachi, G. Y., Electrical properties and sinterability for lithium germanium phosphate $Li_{1+x}M_xGe_{2-x}(PO_4)_3$, M = Al, Cr, Ga, Fe, Sc and In systems. *Bull. Chem. Soc. Jap.*, 1992, **65**, 2200–2204.
18. Aono, H., Sugimoto, E., Sadaoka, Y., Imanaka, N. and Adachi, G. Y., The electrical properties of ceramic electrolytes for $LiM_xTi_{2-x}(PO_4)_3 + y\ Li_2O$, M = Ge, Sn, Hf and Zr systems. *J. Electrochem. Soc.*, 1993, **140**, 1827–1833.
19. Tohge, N., Zhu, J. and Minami, T., Low-temperature preparation of $LiTi_2(PO_4)_3$ by the sol–gel process. *Chem. Express*, 1990, **5**, 973–976.
20. Ando, Y., Hirose, N., Kuwano, J., Kato, M. and Otsuka, H., Preparation of lithium ion conducting solid solutions based on $LiTi_2(PO_4)_3$ by sol–gel method. In *Ceram. Today—Tomorrow's Ceram.*, ed. P. Vincenzini, 1991, pp. 2245–2252.
21. Livage, J., Henry, M. and Sanchez, C., Sol-gel chemistry of transition metal oxides. *Progress in Solid State Chem.*, 1989, **18**, 259–341.
22. Masse, R., Etude des monophosphates du type $M^ITi_2(PO_4)_3$ pour M^I = Li, Ag, K, Rb et Tl. *Bull. Soc. Fr. Min. and Crist.*, 1970, **93**, 500–503.
23. Casciola, M., Costantino, U., Krogh Andersen, I. G. and Krogh Andersen, E., Preparation structural characterization and conductivity of $LiTi_xZr_{2-x}(PO_4)_3$. *Solid State Ionics*, 1990, **37**, 281–287.
24. Alami, M., Brochu, R., Soubeyroux, J. L., Gravereau, P., Le Flem, G. and Hagenmuller, P., Structure and thermal expansion of $LiGe_2(PO_4)_3$. *J. Solid State Chem.*, 1991, **90**, 185–193.
25. Shanon, R. D., Revised effective ionic radii and systematic studies of interatomic distances in halides and chalcogenides. *Acta Cryst.*, 1976, **A32**, 751–767.
26. Delmas, C., Viala, J. C., Olazcuaga, R., Le Flem, G. and Hagenmuller, P., Conductivité ionique dans les systèmes $Na_{1+x}Zr_{2-x}L_x(PO_4)_3$ (L = Cr, Yb). *Mat. Res. Bull.*, 1981, **16**, 83–90.
27. Kleitz, M., Dessemond, L. and Steil, M. C., Model for ion-blocking at internal interfaces in zirconias. *Solid State Ionics*, 1995, **75**, 107–115.
28. Cretin, M., Réalisation et étude de capteurs potentiométriques à membranes céramiques sélectives à l'ion lithium. PhD. thesis, Institut National Polytechnique de Grenoble, France, 1996.
29. Dessemond, L. and Kleitz, M., Effects of mechanical damage on the electrical properties of zirconia ceramics. *J. Eur. Ceram. Soc.*, 1992, **9**, 35–39.
30. Boilot, J. P., Collin, G. and Colomban, P., Relation structure-fast ion conduction in the NASICON solid solution. *J. Solid State Chem.*, 1988, **73**, 160–171.
31. Cretin, M., Khireddine, H. and Fabry, P., NASICON structure for alkaline ion recognition. *Sensors and Actuators B*, 1997, **43**, 224–229.
32. Mauvy, F., Cretin, M., Siebert, E. and Fabry, P., Mechanisms of selectivity in alkali ion sensitive membrane based on NASICON. *J. New Mat. for Electrochem. Syst.*, 1998, **1**, 71–76.